100km Single-ended Distributed Vibration Sensor based on Remotely Pumped EDFA

LIEKE D. VAN PUTTEN[1], ALI MASOUDI[1,*], AND GILBERTO BRAMBILLA[1]

[1] Optoelectronics Research Centre, University of Southampton, Southampton, United Kingdom
[*] Corresponding author: A.Masoudi@soton.ac.uk

Compiled October 21, 2019

In this study, a single-ended distributed vibration sensor with 100km sensing range is reported. This sensing range is achieved by remotely pumping two pieces of Er-doped fibers incorporated along the sensing fiber with a 1480nm Raman fiber laser at the front-end of the fiber. A strain resolution of 100nϵ combined with a spatial resolution of 2.6m is achieved at the far end of the fiber.

OCIS codes: (060.2370) Fiber optics sensors; (120.4825) Optical time domain reflectometry; (290.5870) Scattering, Rayleigh; (120.7280) Vibration analysis

http://dx.doi.org/10.1364/ao.XX.XXXXXX

Distributed optical fiber dynamic strain sensors, also known as distributed vibration sensors (DVS) have been used in a wide range of applications from monitoring the condition of high voltage subsea cables to structural health monitoring of pipelines and mapping terrestrial seismic activities [1–4]. For all these applications, the length of the sensing fiber is of vital importance since a longer sensing range means a larger structure or a wider area can be monitored with a single sensing system. As a result, recent research activities have focused on increasing the sensing range of DVS. In 2014, Wang et al. reported a sensing system with 175km sensing range and 25m spatial resolution, using a hybrid distributed amplification [5]. The proposed setup used a combination of co-pumping second-order Raman amplification and counter-pumping first-order Raman and Brillouin amplification to achieve this sensing range. Similar long-range phase-sensitive optical time-domain reflectometer (ϕ-OTDR) systems based on Raman amplification have also been reported capable of detecting vibrations at distances over 100km [1, 6].

Although all these systems can detect vibrations over a long range, they are not capable of quantify the vibration magnitude. In order to fully quantify the dynamic strains along the sensing fiber, the differential phase of the backscattered Rayleigh light needs to be employed [7]. In 2017, Pastor-Graells et al. have demonstrated a long-range DVS system based on linearly chirped probe pulse with 75km sensing range using bidirectional first-order Raman amplification [8]. This system achieved a 10m spatial resolution and 1nϵ strain resolution. This technique was later combined with time-gated digital optical frequency domain reflectometry (TGD-OFDR) to achieve 108km sensing range with a spatial resolution of 5m and a strain sensitivity of 220p$\epsilon/\sqrt{Hz}$ [9]. However, both techniques required access to both end of the sensing fiber due to the use of bidirectional amplification, a requirement which may not be feasible for some implementations. Recently, Zhang et al. have demonstrated a single-ended DVS with 80km range [10]. This sensing range was achieved through nonlinear modulation of the probe pulse frequency and without the help of distributed amplification. The interrogation setup used to control the pulse chirp, however, was quite elaborate and extracting the strain information required complex signal processing.

To extend the sensing range of DVS systems, a different approach was adopted by Cameron et al. [11]. In this approach, a standard single-mode fiber (SSMF) was spliced to an ultra-low loss (ULL) fiber with 0.155 dB/km attenuation at one end and an enhanced backscattered Fiber (ENHF) at the other end to achieve a maximum sensing range of 125km without the use of inline amplification. However, the study did not disclose the operating principle of the system and the strain sensitivity of the setup. In addition, the spatial resolution of the sensor was limited to 10m.

In 2005, Cho et al. have proposed a technique to increase the sensing range of distributed optical fiber sensors (DOFS) beyond the 50km limit of the first-order Raman in-line amplifiers [12]. In this study, a 1480nm laser was used as both a Raman inline amplifier and a pump for an Erbium-doped fiber that was situated at 50km from the front end of the sensing fiber. Cho et al. showed that by remotely pumping a 2m long Erbium-doped fiber, the sensing range of their Brillouin optical time domain reflectometry (BOTDR) setup could be extended to 88km. In this study, the same concept proposed in Ref [12] is used to demonstrate a single-ended DVS system with 100km sensing range.

The sensing principle of the DVS setup used in this study is based on analysing the phase of the Rayleigh backscattered light from adjacent points on the sensing fiber [13]. Briefly, the variation in the length of a given section of an optical fiber can be measured by analysing the phase difference between the Rayleigh backscattered light from the two ends of that section. The relationship between the phase difference, $\Delta\phi$, and the length, l, is given by [14]:

$$\Delta\phi = 0.78 \times \frac{2\pi n}{\lambda} 2l + (\phi_2 - \phi_1) \quad (1)$$

where n is the refractive index of the fiber, λ is the wavelength of the probe light, and ϕ_1 and ϕ_2 are two random phases from the two ends of the section. Equation 1 shows that the phase-difference is directly proportional to the length of the fiber and any changes in the length or strain of the fiber can be measured by measuring the changes in the phase difference.

In this study, an imbalanced Mach-Zehnder interferometer (IMZI) was used to monitor $\Delta\phi$. The path imbalance of the IMZI creates a temporal shift between the light traveling in its arms. The gauge length of the sensor is determined by the length of the delay fiber in the IMZI. To avoid signal fading, a symmetric 3x3 coupler was used at the output of the IMZI to create three outputs with a phase shift of $2\pi/3$ between them. Using phase demodulation algorithms, the phase shift and, subsequently the dynamic strain can then be measured from the three outputs.

To increase the sensing range of the DVS, two forms of amplifications were utilized. The first form was an in-line Raman optical amplifier. In a Raman optical amplifier, stimulated Raman scattering (SRS) energy from a higher-frequency pump is transmitted to a lower-frequency signals. In this setup, a 1480nm pump was used to amplify 1550nm photons through SRS. Although 1450nm would be the ideal wavelength to use for amplifying 1550nm light, 1480nm laser can also be used due to the broad gain spectrum of Raman amplifiers (the FWHM is around 50nm at 1550nm).

The second form of amplification used was a remotely pumped Erbium-doped fiber amplifier (EDFA). This amplifier was implemented by splicing a short piece of an Er-doped fiber at the end of a long stretch of standard single-mode sensing fiber and pumping it with the residual power from the 1480nm laser.

The experimental setup is shown in Fig. 1. The output of a 1550nm distributed feedback (DFB) laser with 50kHz linewidth was modulated by an electro-optic modulator (EOM) to generate 20ns probe pulse with 4mW peak power. An EDFA (EDFA1) was used to increase the peak power to 100mW. A DWDM filter with 100GHz bandwidth was used to reduce the amplified spontaneous emission (ASE) from EDFA1. The amplified pulse was then picked by an acousto-optic modulator (AOM) with 50dB extinction ratio to eliminate any ASE within the band-pass of the DWDM filter from leaking into the sensing fiber.

The probe pulse with 40mW peak power was combined with 500mW of continuous wave (CW) 1480nm pump at the front-end of the sensing fiber by a 1480nm/1550nm wavelength division multiplexer (WDM) and launched into the sensing fiber. The power of the 1480nm laser pump and the peak power of the probe pulse were adjusted to avoid the onset of non-linear effects such as self-phase modulation [15].

The sensing fiber consisted of seven sections. The first five sections included three SSMF fibers 48km, 25km, and 26km in length joined to one another by 2m and 2.5m of Er-doped fibers. The length of the two Er-doped fibers were chosen to provide 8dB and 9dB amplification, respectively. The end of the last fiber was spliced to a 10m long standard single mode fiber (SMF-28) wrapped around a piezoelectric (PZT) actuator. Finally, the fiber on the PZT was spliced to a 500m long fiber to separate it from the far end of the sensing fiber.

The backscattered Rayleigh light was collected by the circulator C1 and filtered by another DWDM filter with 100GHz bandwidth to remove the majority of Raman backscattered light from the 1480nm pump. The filtered light was then amplified by an optical amplifier (EDFA2) and further filtered by a fiber Bragg grating (FBG) (λ_B=1550.1, $\Delta\lambda$ = 6GHz (0.05nm), reflectivity = 70%) to remove the ASE from the optical amplifier as well as

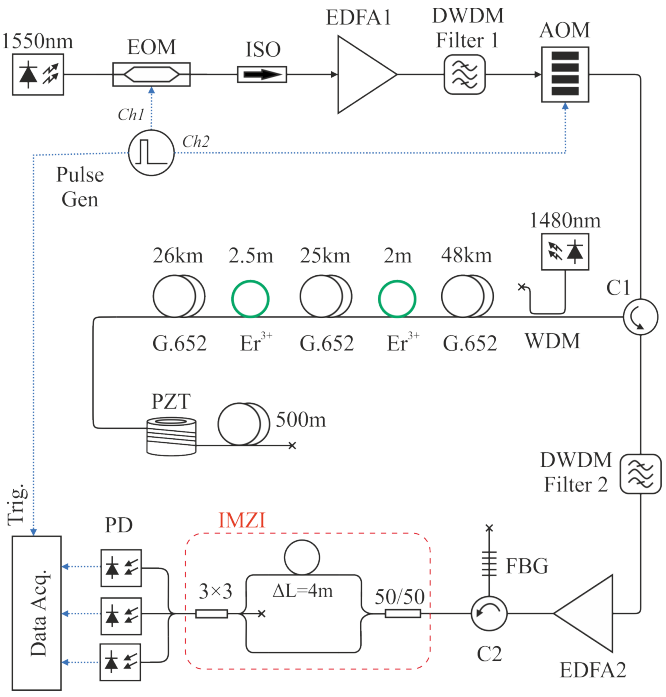

Fig. 1. Experimental setup for a long-range DVS with two remotely pumped EDFAs. EOM: Electro-optic modulator; ISO: Isolator; EDFA: Erbium-doped fiber amplifier, DWDM: Dense wavelength division multiplexing; AOM: Acousto-optic modulator; WDM: Wavelength division multiplexer; PZT: Piezoelectric actuator; FBG: Fiber Bragg grating; C: Circulator; IMZI: Imbalance Mach-Zehnder interferometer; PD: Photodetector.

reducing the contribution of Raman backscattered light. The amplified backscattered light was fed into a thermally insulated Mach-Zehnder interferometer (MZI) with 4m path-imbalance. Three amplified photodetectors (BW = 600MHz, Ω = 80V/mA) were used to sample the backscattered light from the 3×3 coupler at the output of the MZI. The photodetectors were sampled at 625MSa/s with a 1GHz bandwidth digitizer.

Using the attenuation of the SSMF fiber and the absorption of Er-doped fiber at 1480nm, the power of the pump laser before and after both EDFAs was calculated. Table 1 provides an

Table 1. Pump power along the fiber and amplification of the main signal by the two EDFAs

Parameter	Value	Unit
Input Raman Pump Power	500	mW
Fiber loss at 1480nm	0.21	dB/km
Er-doped fiber absorption at 1480nm	5	dB/m
Pump power at 48km	49.1	mW
Pump power after first EDFA	4.9	mW
Pump power at 72km	1.5	mW
Pump power after second EDFA	0.15	mW
First EDFA gain	8	dB
Second EDFA gain	9	dB

overview of the pump power along the fiber and the amplification of the probe signal by the two EDFAs.

In Fig. 2, two OTDR traces are compared. The first (blue) used both Raman amplification and EDFA. For this OTDR trace, the pulse peak power and the 1480nm CW pump power were 40mW and 500mW, respectively. The second OTDR trace (orange) did not have any optical amplification but had a higher launched probe power of 220mW. The launching power was set to 220mW below the threshold of the non-linear effects such as stimulated Raman scattering (SRS), stimulated Brillouin scattering (SBS), and self-phase modulation (SPM). From the trace with optical amplification, three different zones can be identified. The first zone is the first 48km of the fiber, where Raman amplification is used, the second zone which can be identified by the peak at 48km, where the first section of Er-doped fiber is installed, and ends at 73km, and the third zone from the peak at 73km, where the second section of Er-doped fiber is installed, and ends at 100km. Without optical amplification, it can be seen that the power exponentially decays along the fiber and reaches below the level of the amplified trace within 35km, even when a higher power probe pulse is used. From this figure, It can be seen that with the two optical amplifiers, the Rayleigh backscattered signal is clearly visible at 100km. Without the optical amplification, the signal-to-noise ratio fell to unity at approximately 50km for the probe pulse with 220mW launch power.

Fig. 3 shows the results of the processed signals. Fig. 3(a) shows the top view map of the strain level in the time domain. The location of the strain and its periodic profile can be seen in this figure. The colour-bar next to this diagram represents the strain level in $\mu\epsilon$. The fast Fourier transform (FFT) of the strain level is shown in the 3D diagram of Fig. 3(b) where the horizontal axes show the distance and the frequency components of vibrations along the fiber while the vertical axis indicates the magnitude of the vibration. The data used for this FFT was captured over 10 seconds. The peak in this figure corresponds to the location of the perturbation. The magnitude and frequency of the vibration applied by the PZT to the fiber is measured as 0.85 $\mu\epsilon$ and 10Hz, respectively, at the distance of 99.3km from

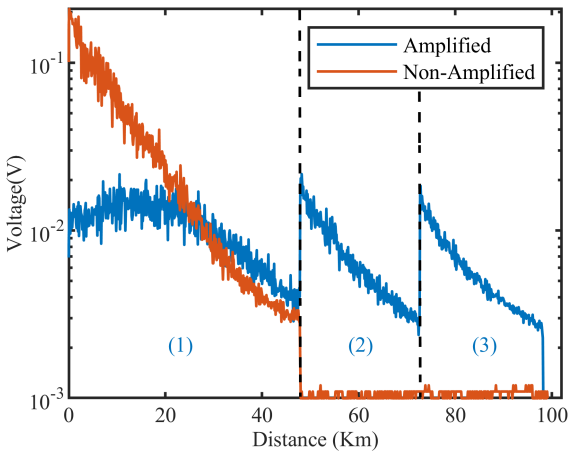

Fig. 2. Measured Rayleigh backscattered signal (blue) with combined EDFA and Raman amplification using a launched power of 40mW combined with a 500mW 1480nm pump; (orange) without the use of optical amplification with 220mW launched power.

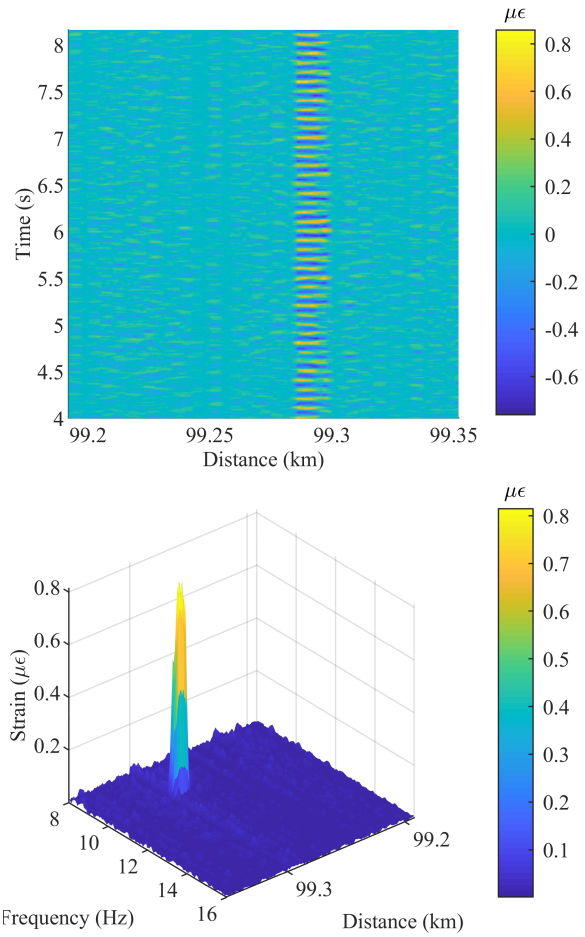

Fig. 3. 3D map of the strain distribution along the sensing fiber as a function of a) time and distance and b) frequency and distance.

the front-end of the sensing fiber.

2D cross-sections of the 3D diagrams in Fig. 3 are shown in Fig. 4. Fig. 4(a) depicts the cross-section of the 3D time-domain plot at 99.3km, showing the strain variation at a fixed point on the fiber as a function of time. The strain is periodic (sinusoidal) and has slight variation in amplitude due to noises in the system such as laser phase noise. The average value of the strain amplitude is 0.85 $\mu\epsilon$. Figure 4(b) shows a 2D cross-section of the frequency domain results at fixed point on the fiber as a function of frequency. This plot can be used to verify the frequency and magnitude of the vibration at a fixed point. It can also be used to measure the noise floor of the setup as a function of frequency at that position. Figure 4(c) depicts a 2D cross-section of the frequency domain plot (Fig. 3(b)) at a fixed frequency as a function of distance. The analysis of this plot demonstrates that the 10/90% spatial resolution of the system is 2.6m which is close to the theoretical limit of 2m. The discrepancy between the theoretical and experimental values of the spatial resolution is due to the temporal and spatial data averaging which was implemented to improve the signal-to-noise ratio (SNR).

Fig. 5 shows the strain level on the fiber measured by the DVS as a function of the input voltage to the PZT. For this test, different strain levels were exerted on the fiber by the PZT at a

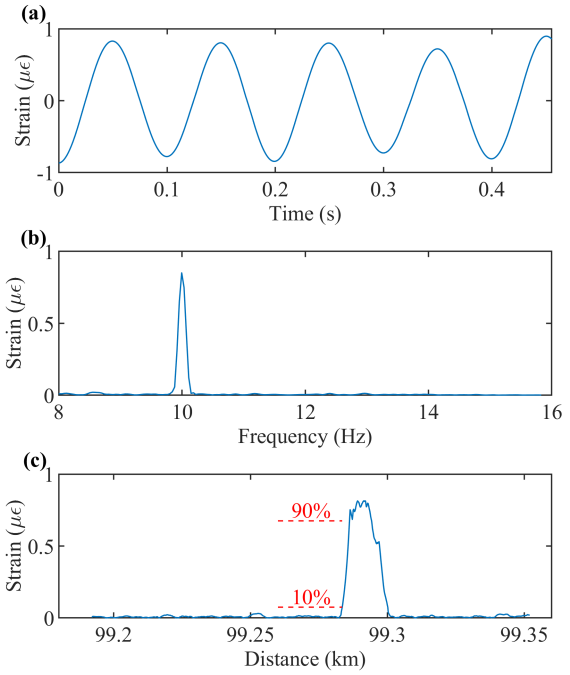

Fig. 4. 2D cross-section of the 3D diagram of Fig. 3 at a specific location on the sensing fiber where strain is applied (99.3km). a) The 2D cross-section in time-domain b) the 2D cross-section in the frequency-domain at fixed position on the fiber and c) 2D cross-section in the frequency-domain at fixed frequency.

fixed frequency. This figure shows a linear relationship between the applied and measured strain on the sensing fiber. Due to the laser phase noise, drift in IMZI path-imbalance, detector noise, and digitization level of the data acquisition card used in the setup, the minimum detectable strain at 99.3km was measured to be 100nϵ for a 10Hz oscillation corresponding to a power spectral density (PSD) noise of $7n\epsilon/\sqrt{Hz}$ within 5Hz to 500Hz frequency band. It should be pointed out that the noise floor of the sensing system depends on the amplitude of the coherent Rayleigh noise (CRN). The sections of the OTDR trace where the amplitude of the CRN is closer to zero has higher noise level since the phase demodulation algorithm rely on weak backscattered light to extract the phase information. The $100n\epsilon$ noise floor reported in this study was obtained by analysing the strain level at unperturbed section of the sensing fiber. By comparing the strain response profile of the PZT at 10Hz which was measured separately, it can be concluded that the proposed sensing arrangement is capable of quantifying the frequency, amplitude, and location of dynamic perturbations anywhere along a 100km long sensing fiber.

In summary, a long range distributed vibration sensor with in-line Raman amplification and remotely pumped EDFA is demonstrated. It was shown that by combining these two amplification techniques, the DVS system can accurately measure the location, frequency, and amplitude of the perturbation applied to the sensing fiber at the far-end of the 100km long SSMF from a single end of the fiber. The system showed a spatial and strain resolution of 2.6m and 100nϵ, respectively.

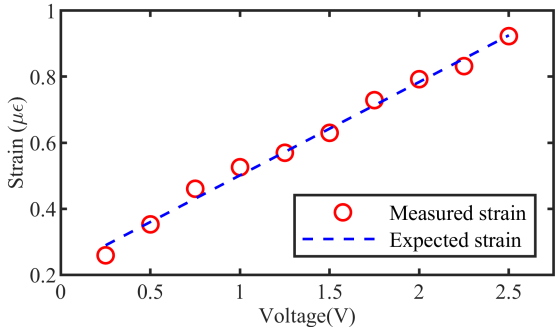

Fig. 5. Strain response of the fiber to the PZT input voltage for 10Hz sinusoidal signal measured by the DVS.

1. FUNDING INFORMATION

Engineering and Physical Sciences Research Council (EPSRC) - (EP/N00437X/1); Natural Environment Research Council (NERC) - (NE/S012877/1); Royal Society - (CHL/R1/180350) All the data supporting this study are openly available from the University of Southampton repository at https://doi.org/10.5258/SOTON/D1116.

REFERENCES

1. F. Peng, H. Wu, X.-H. Jia, Y.-J. Rao, Z.-N. Wang, and Z.-P. Peng, Opt. Express **22**, 13804 (2014).
2. A. Masoudi, J. A. Pilgrim, T. P. Newson, and G. Brambilla, J. Light. Technol. **37**, 1352 (2019).
3. S. Dou, N. Lindsey, A. M. Wagner, T. M. Daley, B. Freifeld, M. Robertson, J. Peterson, C. Ulrich, E. R. Martin, and J. B. Ajo-Franklin, Sci. reports **7**, 11620 (2017).
4. P. Jousset, T. Reinsch, T. Ryberg, H. Blanck, A. Clarke, R. Aghayev, G. P. Hersir, J. Henninges, M. Weber, and C. M. Krawczyk, Nat. communications **9**, 2509 (2018).
5. Z. N. Wang, J. J. Zeng, J. Li, M. Q. Fan, H. Wu, F. Peng, L. Zhang, Y. Zhou, and Y. J. Rao, Opt. Lett. **39**, 5866 (2014).
6. H. F. Martins, S. Martin-Lopez, P. Corredera, M. L. Filograno, O. Frazao, and M. Gonzalez-Herraez, J. Light. Technol. **32**, 1510 (2014).
7. A. Masoudi and T. P. Newson, Rev. Sci. Instruments **87**, 011501 (2016).
8. J. Pastor-Graells, J. Nuno, M. R. Fernandez-Ruiz, A. Garcia-Ruiz, H. F. Martins, S. Martin-Lopez, and M. Gonzalez-Herraez, J. Light. Technol. **35**, 4677 (2017).
9. D. Chen, Q. Liu, and Z. He, J. Light. Technol. **37**, 4462 (2019).
10. J. Zhang, H. Wu, H. Zheng, J. Huang, G. Yin, T. Zhu, F. Qiu, X. Huang, D. Qu, and Y. Bai, J. Light. Technol. **17**, 1 (2019).
11. G. Cedilnik, G. Lees, P. Erik Schmidt, S. Herstrøm, and T. Geisler, IEEE Sensors Lett. **3**, 1 (2019).
12. Y. T. Cho, M. N. Alahbabi, G. Brambilla, and T. P. Newson, IEEE Photon. Technol. Lett. **17**, 1256 (2005).
13. A. Masoudi and T. P. Newson, Opt. Express **25**, 32021 (2017).
14. M. Chen, A. Masoudi, and G. Brambilla, Opt. Express **27**, 9684 (2019).
15. H. F. Martins, S. Martin-Lopez, P. Corredera, P. Salgado, O. Frazao, and M. González-Herráez, Opt. Lett. **38**, 872 (2013).

FULL REFERENCES

1. F. Peng, H. Wu, X.-H. Jia, Y.-J. Rao, Z.-N. Wang, and Z.-P. Peng, "Ultra-long high-sensitivity ϕ-otdr for high spatial resolution intrusion detection of pipelines," Opt. Express **22**, 13804–13810 (2014).
2. A. Masoudi, J. A. Pilgrim, T. P. Newson, and G. Brambilla, "Subsea cable condition monitoring with distributed optical fiber vibration sensor," J. Light. Technol. **37**, 1352–1358 (2019).
3. S. Dou, N. Lindsey, A. M. Wagner, T. M. Daley, B. Freifeld, M. Robertson, J. Peterson, C. Ulrich, E. R. Martin, and J. B. Ajo-Franklin, "Distributed acoustic sensing for seismic monitoring of the near surface: A traffic-noise interferometry case study," Sci. reports **7**, 11620 (2017).
4. P. Jousset, T. Reinsch, T. Ryberg, H. Blanck, A. Clarke, R. Aghayev, G. P. Hersir, J. Henninges, M. Weber, and C. M. Krawczyk, "Dynamic strain determination using fibre-optic cables allows imaging of seismological and structural features," Nat. communications **9**, 2509 (2018).
5. Z. N. Wang, J. J. Zeng, J. Li, M. Q. Fan, H. Wu, F. Peng, L. Zhang, Y. Zhou, and Y. J. Rao, "Ultra-long phase-sensitive otdr with hybrid distributed amplification," Opt. Lett. **39**, 5866–5869 (2014).
6. H. F. Martins, S. Martin-Lopez, P. Corredera, M. L. Filograno, O. Frazao, and M. Gonzalez-Herraez, "Phase-sensitive optical time domain reflectometer assisted by first-order raman amplification for distributed vibration sensing over >100 km," J. Light. Technol. **32**, 1510–1518 (2014).
7. A. Masoudi and T. P. Newson, "Contributed review: Distributed optical fibre dynamic strain sensing," Rev. Sci. Instruments **87**, 011501 (2016).
8. J. Pastor-Graells, J. Nuno, M. R. Fernandez-Ruiz, A. Garcia-Ruiz, H. F. Martins, S. Martin-Lopez, and M. Gonzalez-Herraez, "Chirped-pulse phase-sensitive reflectometer assisted by first-order raman amplification," J. Light. Technol. **35**, 4677–4683 (2017).
9. D. Chen, Q. Liu, and Z. He, "108-km distributed acoustic sensor with $220 - p\epsilon/\sqrt{Hz}$ strain resolution and 5-m spatial resolution," J. Light. Technol. **37**, 4462–4468 (2019).
10. J. Zhang, H. Wu, H. Zheng, J. Huang, G. Yin, T. Zhu, F. Qiu, X. Huang, D. Qu, and Y. Bai, "80 km fading free phase-sensitive reflectometry based on multi-carrier nlfm pulse without distributed amplification," J. Light. Technol. **17**, 1–1 (2019).
11. G. Cedilnik, G. Lees, P. Erik Schmidt, S. Herstrøm, and T. Geisler, "Pushing the reach of fiber distributed acoustic sensing to 125 km without the use of amplification," IEEE Sensors Lett. **3**, 1–1 (2019).
12. Y. T. Cho, M. N. Alahbabi, G. Brambilla, and T. P. Newson, "Distributed raman amplification combined with a remotely pumped edfa utilized to enhance the performance of spontaneous brillouin-based distributed temperature sensors," IEEE Photon. Technol. Lett. **17**, 1256–1258 (2005).
13. A. Masoudi and T. P. Newson, "Analysis of distributed optical fibre acoustic sensors through numerical modelling," Opt. Express **25**, 32021–32040 (2017).
14. M. Chen, A. Masoudi, and G. Brambilla, "Performance analysis of distributed optical fiber acoustic sensors based on ϕ-otdr," Opt. Express **27**, 9684–9695 (2019).
15. H. F. Martins, S. Martin-Lopez, P. Corredera, P. Salgado, O. Frazao, and M. González-Herráez, "Modulation instability-induced fading in phase-sensitive optical time-domain reflectometry," Opt. Lett. **38**, 872–874 (2013).